Results on best theories for metallic and laminated shells including Layer-Wise models.

E. Carrera[a,b]*, M. Cinefra[a]†, A. Lamberti[a]‡, M. Petrolo[b]§

[a]Department of Mechanical and Aerospace Engineering, Politecnico di Torino,
Corso Duca degli Abruzzi 24, 10129 Torino, Italy
[b]School of Aerospace, Mechanical and Manufacturing Engineering, RMIT University,
PO Box 71, Bundoora VIC 3083, Australia

Submitted to:

Composite Structures

Author for correspondence:

E. Carrera, Professor of Aerospace Structures and Aeroelasticity,
Department of Mechanical and Aerospace Engineering,
Politecnico di Torino,
Corso Duca degli Abruzzi 24,
10129 Torino, Italy,
tel: +39 011 090 6871,
fax: +39 011 090 6899,
e-mail: erasmo.carrera@polito.it,
website: www.mul2.com

*Professor of Aerospace Structures and Aeroelasticity, e-mail: erasmo.carrera@polito.it
†Research Assistant, e-mail: maria.cinefra@polito.it
‡PhD Student, e-mail: alessando.lamberti@polito.it
§Research Fellow, e-mail: marco.petrolo@rmit.edu.au

Abstract

This paper deals with Best Theory Diagrams (BTDs) for metallic and laminated shells. The BTD is a curve that is defined over a 2D reference frame in which the horizontal axis indicates the error of a shell model with respect to a reference solution whereas the vertical axis indicates the number of displacement variables of the model. The best reduced model is a refined model that offers the lowest possible error for a given number of variables. The relevant terms of a model are detected by means of the axiomatic/asymptotic method (AAM), and the error is related to a given variable with respect to an exact or quasi-exact solution. In this work, a genetic algorithm has been used to obtain the BTD. The Carrera Unified Formulation (CUF) has been employed to build the refined models. The CUF makes it possible to generate automatically, and in a unified manner, any plate or shell models. Equivalent Single Layer (ESL) and Layer Wise (LW) refined models have been considered. The governing equations for shells have been obtained through the Principle of Virtual Displacement (PVD), and Navier-type closed form solutions have been considered. BTDs have been constructed by considering the influence of several parameters, such as various geometries, material properties, layouts, different displacement/stress components and loadings. The accuracies of some well-known theories have been evaluated and compared with BTD reduced models. The results suggest that, since the BTD depends on the problem characteristics to a great extent, the systematic adoption of the CUF and the AAM can be considered as a powerful tool to evaluate the accuracy of any structural theory against a reference solution for any structural problem.

1 Introduction

Laminated composite and metallic shells are widely employed in several structural engineering applications, and many mathematical models have been developed over the last decades for the structural analysis of plates and shells. The solution of the 3D elasticity equations can be computationally prohibitive and valid only for a few geometries, material characteristics and boundary conditions. Computationally cheaper 2D structural models are commonly used to analyse shells and plates. The first model that was developed was the Kirchoff-Love ([1], [2]). According to this model, transverse shear and normal strains are assumed to be negligible with respect to the other stress and strain components. An extension of this model to multilayered structures is referred to as the Classical Lamination Theory (CLT). Further details on shell theories can be found in [3].

The inclusion of shear effects can be carried out according to the Reissner-Mindlin model [4, 5] that leads to the First Order Shear Deformation Theory (FSDT). Further refinements of the FSDT can be obtained through the Vlasov model and the Reddy-Vlasov model [6, 7] to account for the homogeneous conditions for the transverse shear stresses at the top and bottom shell/plate surfaces.

A refined model that accounts for both the transverse shear and normal stress effects, i.e. that fulfills Koiter's recommendation [8], was developed by Hildebrand, Reissner and Thomas [9]. Other significant contributions on laminated shell models can be found in [10, 11, 12, 13, 14, 15, 16, 17].

The number of unknown variables in the theories that were mentioned above is independent of the number of layers. These theories are commonly referred to as Equivalent Single Layer Models (ESL). An alternative method is the Layer-Wise (LW) approach [18, 19, 20, 21, 22, 23] in which each layer is seen as an independent plate and compatibility of displacement components

are imposed at the interfaces. In an LW model, the number of unknown variables depends on the number of layers.

Multilayered structures are transversely anisotropic, and the mechanical properties are discontinuous along the thickness. These characteristics lead to transverse displacements whose slopes can rapidly change at the layer interfaces, and transversely discontinuous in-plane stresses. Due to equilibrium conditions, transverse stresses must be continuous at the interfaces. Zig-zag models [24, 25] and mixed variational tools [26, 27, 28] have been developed over the last decades in which the displacement and stress fields can be assumed in each layer. Compatibility and equilibrium conditions are then used at the interfaces to reduce the number of the unknown variables.

The present paper deals with refined shell models that are built by means of the Carrera Unified Formulation (CUF)[29]. According to the CUF, the displacement field of shells and plates can be defined as an arbitrary expansion of the thickness coordinate. The expansion order is a free parameter of the analysis, and it can be chosen via a convergence analysis. The governing equations are obtained through a set of fundamental nuclei whose form does not depend on either the expansion order nor the choices made for the base functions.

In the CUF framework, a novel axiomatic/asymptotic method (AAM) has been recently developed for beams [30, 31] and plates [32, 33]. AAM allows us to investigate the effectiveness of each generalized displacement variable in detecting the solution for a given problem and different values of typical parameters such as the thickness, the orthotropic ratio and the stacking sequence. By retrieving only those variables that play a role in the detection of the mechanical behavior of the structure, this method leads to the definition of reduced models that have the same accuracy of the full model but that have fewer unknown variables. Another important outcome that stemmed from the use of the axiomatic/asymptotic approach was the best theory diagram (BTD) [34]. The BTD is a diagram in which, for a given problem, the computationally

cheapest structural model for a given accuracy can be read. The BTD is influenced by a number of geometrical and material parameters, and it can be obtained by exploiting genetic algorithms [35]. The most recent developments have dealt with the definition of more accurate techniques to evaluate the accuracy of the model [36, 37] and with layer-wise plate models [38].

In this work, BTDs are obtained for metallic and laminated shells through genetic algorithms. Navier-like closed-form solutions are employed, and both ESL and LW models are considered. This paper is a companion work of [39] in which refined plate models were considered. This paper is organized as follows: the geometrical relations for shells and the constitutive equations for laminated structures are presented in Section 2; the CUF is presented in Section 3; the governing equations are introduced in Section 4; the axiomatic/asymptotic technique and the BTD are introduced in Section 5; the results are given in Section 6; the conclusions are drawn in Section 7.

2 Geometrical and constitutive relations for shells

This section deals with the basic geometrical and constitutive equations for multilayered shells. A more complete and detailed description of these equations can be found in [40]. The geometrical parameters and the reference frame of a generic k-layer of a multilayered shell are depicted in Fig. 1. The reference surface is defined as Ω_k, and its boundary is Γ_k. The reference system is defined by α_k, β_k, z_z, and the curvature radii along the principal directions are R_α^k and R_β^k. The following relation are valid in the given orthogonal system of curvilinear coordinates for the square of a line element, the area of an infinitesimal rectangle on Ω_k, and for an infinitesimal

volume, respectively,

$$\begin{aligned} ds_k^2 =& H_\alpha^k d\alpha_k^2 + H_\beta^k d\beta_k^2 + H_z^k dz_k^2 \\ d\Omega_k =& H_\alpha^k \, H_\beta^k \, d\alpha_k \, d\beta_k \\ dV_k =& H_\alpha^k \, H_\beta^k \, H_z^k \, d\alpha_k \, d\beta_k \, dz_k \end{aligned} \tag{1}$$

where

$$H_\alpha^k = A_k \left(1 + \frac{z_k}{R_\alpha^k}\right) \qquad H_\beta^k = B_k \left(1 + \frac{z_k}{R_\beta^k}\right) \qquad H_z^k = 1 \tag{2}$$

Constant curvature shells were considered in this paper; that is, $A_k = B_k = 1$. For the sake of convenience, strain components were grouped into in-plane and out-of-plane components,

$$\boldsymbol{\epsilon}_p^k = [\epsilon_{\alpha\alpha} \;\; \epsilon_{\beta\beta} \;\; \epsilon_{\alpha\beta}] \qquad \boldsymbol{\epsilon}_n^k = [\epsilon_{\alpha z} \;\; \epsilon_{\beta z} \;\; \epsilon_{zz}] \tag{3}$$

and the strain-displacement relations were expressed as (see [3])

$$\begin{aligned} \boldsymbol{\epsilon}_p^k =& \mathbf{D}_p \mathbf{u}^k + \mathbf{A}_p \mathbf{u}^k \\ \boldsymbol{\epsilon}_n^k =& \mathbf{D}_n \mathbf{u}^k + \mathbf{A}_n \mathbf{u}^k = \mathbf{D}_{n\Omega} \mathbf{u}^k + \mathbf{D}_{nz} \mathbf{u}^k + \mathbf{A}_n \mathbf{u}^k \end{aligned} \tag{4}$$

where

$$\mathbf{D}_p = \begin{bmatrix} \frac{\partial_{\alpha_k}}{H_\alpha^k} & 0 & 0 \\ 0 & \frac{\partial_{\beta k}}{H_\beta^k} & 0 \\ \frac{\partial_{\beta k}}{H_\beta^k} & \frac{\partial_{\alpha_k}}{H_\alpha^k} & 0 \end{bmatrix} \qquad \mathbf{A}_p = \begin{bmatrix} 0 & 0 & \frac{1}{H_\alpha^k \, R_\alpha^k} \\ 0 & 0 & \frac{1}{H_\beta^k \, R_\beta^k} \\ 0 & 0 & 0 \end{bmatrix} \tag{5}$$

$$\mathbf{D}_{n\Omega} = \begin{bmatrix} 0 & 0 & \frac{\partial_{\alpha_k}}{H_\alpha^k} \\ 0 & 0 & \frac{\partial_{\alpha_k}}{H_\alpha^k} \\ 0 & 0 & 0 \end{bmatrix} \qquad \mathbf{A}_n = \begin{bmatrix} -\frac{1}{H_\alpha^k \, R_\alpha^k} & 0 & 0 \\ 0 & -\frac{1}{H_\beta^k \, R_\beta^k} & 0 \\ 0 & 0 & 0 \end{bmatrix} \qquad \mathbf{D}_{nz} = \begin{bmatrix} \partial_z & 0 & 0 \\ 0 & \partial_z & 0 \\ 0 & 0 & \partial_z \end{bmatrix} \tag{6}$$

Stress and strain are related by means of the following constitutive equation:

$$\boldsymbol{\sigma}^k = \mathbf{C}^k \, \boldsymbol{\epsilon}^k \tag{7}$$

where $\boldsymbol{\sigma}^k$ is the stress vector of the generic k layer of the shell and $\boldsymbol{\epsilon}^k$ is the strain vector of the generic k layer of the shell. The material elastic coefficients are expressed in the problem reference system. The dependence of the elastic coefficients $\tilde{C}_{ij}$ on Young's modulus, Poisson's ratio, the shear modulus and the fiber angle is not reported here for the sake of brevity, these relations can be found in Reddy's book [7]. Coherently with the strain grouping in Eq. 3, the constitutive equations can be written as

$$\begin{bmatrix} \boldsymbol{\sigma}_p^k \\ \boldsymbol{\sigma}_n^k \end{bmatrix} = \begin{bmatrix} \tilde{\mathbf{C}}_{pp}^k & \tilde{\mathbf{C}}_{pn}^k \\ \tilde{\mathbf{C}}_{np}^k & \tilde{\mathbf{C}}_{nn}^k \end{bmatrix} \cdot \begin{bmatrix} \boldsymbol{\epsilon}_p^k \\ \boldsymbol{\epsilon}_n^k \end{bmatrix} \tag{8}$$

where

$$\boldsymbol{\sigma}_p^k = [\sigma_{\alpha\alpha} \;\; \sigma_{\beta\beta} \;\; \sigma_{\alpha\beta}] \qquad \boldsymbol{\sigma}_n^k = [\sigma_{\alpha z} \;\; \sigma_{\beta z} \;\; \sigma_{zz}] \tag{9}$$

and

$$\mathbf{C}_{pp}^k = \begin{bmatrix} \tilde{C}_{11}^k & \tilde{C}_{12}^k & \tilde{C}_{16}^k \\ \tilde{C}_{21}^k & \tilde{C}_{22}^k & \tilde{C}_{26}^k \\ \tilde{C}_{31}^k & \tilde{C}_{32}^k & \tilde{C}_{66}^k \end{bmatrix} \qquad \mathbf{C}_{pn}^k = \mathbf{C}_{np}^{k^T} = \begin{bmatrix} 0 & 0 & \tilde{C}_{13}^k \\ 0 & 0 & \tilde{C}_{23}^k \\ 0 & 0 & \tilde{C}_{36}^k \end{bmatrix} \qquad \mathbf{C}_{nn}^k = \begin{bmatrix} \tilde{C}_{44}^k & \tilde{C}_{45}^k & 0 \\ \tilde{C}_{45}^k & \tilde{C}_{55}^k & 0 \\ 0 & 0 & \tilde{C}_{33}^k \end{bmatrix} \tag{10}$$

3 Carrera Unified Formulation for shells

In the framework of the CUF, the displacement field above a generic k-layer of a shell can be described as

$$\mathbf{u}^k(\alpha_k, \beta_k, z) = F_\tau(z) \cdot \mathbf{u}^k_\tau(\alpha_k, \beta_k) \qquad \tau = 1, 2, \ldots, M \tag{11}$$

where $\mathbf{u}^k$ is the displacement vector $(u^k_\alpha \; u^k_\beta \; u^k_z)$, F_τ are the expansion functions, $\mathbf{u}^k_\tau = (u^k_{\alpha\tau}, \; u^k_{\beta\tau}, \; u^k_{z\tau})$ are the displacement variables, and M is the total number of expansion terms. M can be chosen arbitrarily. Functions F_τ are most commonly polynomials, but other types of functions could be used, e.g. exponentials, harmonics, etc.. In this paper, ESL and LW were adopted. In the ESL, the expansion functions are defined on the entire thickness. On the other hand, in LW the expansion functions are defined for each layer k. Examples of ESL and LW schemes are shown in Fig.s 2(a) and 2(b) in which a generic displacement component distribution along the thickness is presented according to linear and higher-order expansions.

3.1 Equivalent Single Layer models

Mc-Laurin polynomials were adopted as expansion functions of the thickness coordinate to deal with ESL,

$$F_\tau = z^{\tau-1}, \qquad \tau = 1, 2, \ldots, N+1 \tag{12}$$

where N is the order of the expansion. As in previous CUF works, the ESL models are indicated as EDN, where N is the expansion order. The ED4 model displacement field, for instance, is given by

$$\begin{aligned} u_\alpha &= u_{\alpha_1} + z\, u_{\alpha_2} + z^2\, u_{\alpha_3} + z^3\, u_{\alpha_4} + z^4\, u_{\alpha_5} \\ u_\beta &= u_{\beta_1} + z\, u_{\beta_2} + z^2\, u_{\beta_3} + z^3\, u_{\beta_4} + z^4\, u_{\beta_5} \\ u_z &= u_{z_1} + z\, u_{z_2} + z^2\, u_{z_3} + z^3\, u_{z_4} + z^4\, u_{z_5} \end{aligned} \tag{13}$$

This model has 15 generalized displacement variables. Classical models such as CLT and FSDT can be considered as special cases of the full linear expansion (ED1). For instance, the FSDT model is given by

$$\begin{aligned} u_\alpha &= u_{\alpha_1} + z\, u_{\alpha_2} \\ u_\beta &= u_{\beta_1} + z\, u_{\beta_2} \\ u_z &= u_{z_1} \end{aligned} \tag{14}$$

Poisson's locking is corrected as in [41] in all those models that have first-order displacement fields.

In this paper, many results were compared with those obtained via the model proposed by Pandya (see [42]) in which the displacement components are the following:

$$\begin{aligned} u_\alpha &= u_{\alpha 1} + z\; u_{\alpha 2} + z^2\; u_{\alpha 3} + z^3\; u_{\alpha 4} \\ u_\beta &= u_{\beta 1} + z\; u_{\beta 2} + z^2\; u_{\beta 3} + z^3\; u_{\beta 4} \\ u_z &= u_{z1} \end{aligned} \tag{15}$$

3.2 Layer Wise models

LW models can be conveniently built by using Legendre's polynomials as expansion functions along each layer. According to CUF, the LW displacement field can be written as

$$\mathbf{u}^k = F_t \cdot \mathbf{u}_t^k + F_b \cdot \mathbf{u}_b^k + F_r \cdot \mathbf{u}_r^k = F_\tau \mathbf{u}_\tau^k \qquad \tau = t, b, r \;\; r = 2, 3, \ldots, N \qquad k = 1, 2, \ldots, N_l \tag{16}$$

where N_l indicates the number of the layers. The subscripts t and b denote those values at the top and at the bottom of the layer, respectively. The Legendre polynomials for a fourth-order model are the following:

$$P_0 = 1 \quad P_1 = \zeta_k \quad P_2 = \frac{3\zeta_k^2 - 1}{2} \quad P_3 = \frac{5\zeta_k^3 - 3\zeta_k}{2} \quad P_4 = \frac{35\zeta_k^4}{8} - \frac{15\zeta_k^2}{4} + \frac{3}{8} \tag{17}$$

where ζ_k is the adimensional thickness coordinate, $-1 \leq \zeta_k \leq 1$. The F_τ functions are obtained from the Legendre polynomials as follows:

$$F_t = \frac{P_0 + P_1}{2} \qquad F_b = \frac{P_0 - P_1}{2} \qquad F_r = P_r - P_{r-2} \qquad r = 2, 3, \ldots, N \tag{18}$$

LW models are referred to as LDN, where N is the expansion order. The LD4 model, for instance, is based on the following displacement field:

$$\begin{aligned} u^k_\alpha &= F_t\, u^k_{\alpha t} + F_2\, u^k_{\alpha 2} + F_3\, u^k_{\alpha 3} + F_4\, u^k_{\alpha 4} + F_b\, u^k_{\alpha b} \\ u^k_\beta &= F_t\, u^k_{\beta t} + F_2\, u^k_{\beta 2} + F_3\, u^k_{\beta 3} + F_4\, u^k_{\beta 4} + F_b\, u^k_{\beta b} \\ u^k_z &= F_t\, u^k_{z t} + F_2\, u^k_{z 2} + F_3\, u^k_{z 3} + F_4\, u^k_{z 4} + F_b\, u^k_{z b} \end{aligned} \tag{19}$$

A more detailed description of CUF shell models can be found in [43, 44].

4 Governing equations

The Principle of Virtual Displacements (PVD) was used to obtain the governing equations,

$$\delta L_{int} = \delta L_{ext} \tag{20}$$

where δL_{int} is the virtual variation of the internal work and δL_{ext} is the virtual variation of the external work. The PVD can be written as

$$\sum_{k=1}^{N_l} \int_{\Omega_k} \int_{A_k} \left(\delta \boldsymbol{\epsilon}_p^{k^T} \boldsymbol{\sigma}_p^k + \delta \boldsymbol{\epsilon}_n^{k^T} \boldsymbol{\sigma}_n^k \right) dz\, d\Omega_k = \sum_{k=1}^{N_l} \delta L^k_{ext} \tag{21}$$

Further details about the CUF and its implementation through the use of variational principles can be found in [44].

The governing equations can be written as

$$\delta \mathbf{u}_s^k : \ \mathbf{K}_d^{k\tau s} \cdot \mathbf{u}_\tau^k = \mathbf{P}_\tau^k \tag{22}$$

and the boundary conditions are

$$\mathbf{\Pi}_d^{k\tau s} \mathbf{u}_\tau^k = \mathbf{\Pi}_d^{k\tau s} \overline{u}_\tau^k \tag{23}$$

where $\mathbf{P}_\tau^k$ is the external load. The fundamental nucleus, $\mathbf{K}_d^{\tau s}$ is assembled through the indexes τ and s. Superscript k denotes the assembly at the layer level. The explicit form of the fundamental nucleus is

$$\begin{aligned}
\mathbf{K}_d^{k\tau\, s} = \Big\{ & (-\mathbf{D}_p + \mathbf{A}_p)^T \left[\mathbf{C}_{pp}^k E_{s\tau}\, \mathbf{D}_p + \mathbf{C}_{pp}^k E_{s\tau}\, \mathbf{A}_p + \mathbf{C}_{pn}^k E_{s\tau} \mathbf{D}_{n\Omega} + \mathbf{C}_{pn}^k E_{s\tau_{,z}} + \mathbf{C}_{pn}^k E_{s\tau} \mathbf{A}_n \right] \\
& + (-\mathbf{D}_{n\Omega} + \mathbf{A}_n)^T \left[\mathbf{C}_{pn}^{kT} E_{s\tau} \mathbf{D}_p + \mathbf{C}_{pn}^{kT} E_{s\tau} \mathbf{A}_p + \mathbf{C}_{nn}^k E_{s\tau} \mathbf{D}_{n\Omega} + \mathbf{C}_{nn}^k E_{s\tau} \mathbf{A}_n + \mathbf{C}_{nn}^k E_{s\tau_{,z}} \right] \\
& + \left[\mathbf{C}_{pn}^{kT} E_{s_{,z}\tau} \mathbf{D}_p + \mathbf{C}_{pn}^{kT} E_{s_{,z}\tau} \mathbf{A}_p + \mathbf{C}_{nn}^k E_{s_{,z}\tau} \mathbf{D}_{n\Omega} + \mathbf{C}_{nn}^k E_{s_{,z}\tau} \mathbf{A}_n + \mathbf{C}_{nn}^k E_{s_{,z}\tau_{,z}} \right] \Big\}\, H_\alpha^k\, H_\beta^k
\end{aligned} \tag{24}$$

and for the boundary conditions it is

$$\begin{aligned}
\mathbf{\Pi}_d^{k\,\tau\, s} = \Big\{ & (\mathbf{I}_p)^T \left[\mathbf{C}_{pp}^k E_{s\tau}\, \mathbf{D}_p + \mathbf{C}_{pp}^k E_{s\tau}\, \mathbf{A}_p + \mathbf{C}_{pn}^k E_{s\tau} \mathbf{D}_{n\Omega} + \mathbf{C}_{pn}^k E_{s\tau} \mathbf{A}_n + \mathbf{C}_{pn}^k E_{s\tau_{,z}} \right] \\
& + (\mathbf{I}_{n\Omega})^T \left[\mathbf{C}_{pn}^{kT} E_{s\tau} \mathbf{D}_p + \mathbf{C}_{pn}^{kT} E_{s\tau} \mathbf{A}_p + \mathbf{C}_{nn}^k E_{s\tau} \mathbf{D}_{n\Omega} + \mathbf{C}_{nn}^k E_{s\tau} \mathbf{A}_n + \mathbf{C}_{nn}^k E_{s\tau_{,z}} \right] \Big\}\, H_\alpha^k\, H_\beta^k
\end{aligned} \tag{25}$$

The following additional matrices have been introduced:

$$\mathbf{I}_p = \begin{bmatrix} \frac{1}{H_\alpha^k} & 0 & 0 \\ 0 & \frac{1}{H_\beta^k} & 0 \\ \frac{1}{H_\beta^k} & \frac{1}{H_\alpha^k} & 0 \end{bmatrix} \qquad \mathbf{I}_{np} = \begin{bmatrix} 0 & 0 & \frac{1}{H_\alpha^k} \\ 0 & 0 & \frac{1}{H_\beta^k} \\ 0 & 0 & 0 \end{bmatrix} \tag{26}$$

and

$$\left(E_{s\tau}, E_{s\tau,z}, E_{s\tau,z}, E_{s\tau}, E_{s,z\tau,z}\right) = \int_{A_k} \left(F_s\, F_\tau, F_s F_{\tau,z}\, F_{s,z} F_\tau, F_{s,z} F_{\tau,z}\right) dz \tag{27}$$

The analyses herein reported were based on the Navier closed-form solution for simply supported orthotropic shells, loaded by a transverse distribution of harmonic loadings. The following properties hold

$$\tilde{C}_{pp16} = \tilde{C}_{pp26} = \tilde{C}_{pn36} = \tilde{C}_{nn45} = 0 \tag{28}$$

The terms $\mathbf{u}_\tau^k$ for an LW model are expressed as:

$$\begin{aligned} u_{\alpha_\tau}^k &= \textstyle\sum_{m,n} \hat{U}_{\alpha_\tau}^k \cdot \cos\left(\frac{m\pi\alpha_k}{a_k}\right) \sin\left(\frac{n\pi\beta_k}{b_k}\right) \qquad k = 1, N_l \\ u_{\beta_\tau}^k &= \textstyle\sum_{m,n} \hat{U}_{\beta_\tau}^k \cdot \sin\left(\frac{m\pi\alpha_k}{a_k}\right) \cos\left(\frac{n\pi\beta_k}{b_k}\right) \qquad \tau = 1, M \\ u_{z_\tau}^k &= \textstyle\sum_{m,n} \hat{U}_{z_\tau}^k \cdot \sin\left(\frac{m\pi\alpha_k}{a_k}\right) \sin\left(\frac{n\pi\beta_k}{b_k}\right) \qquad m, n \in \mathbb{N} \end{aligned} \tag{29}$$

where $\hat{U}_{\alpha_\tau}^k$, $\hat{U}_{\beta_\tau}^k$ and $\hat{U}_{z_\tau}^k$ are the amplitudes, m and n are the numbers of waves (they range from 0 to ∞) and a_k and b_k are the shell lengths in the α_k and β_k directions, respectively. The same solution can be applied to the ESL approach, in this case the displacement variables appear without the superscript k.

5 The axiomatic/asymptotic method and the Best Theory Diagram

Structural analyses can be carried out by means of models with different accuracies. In general, better accuracies can be obtained by increasing the order of the expansion; that is, by increasing the number of unknown variables. The axiomatic/asymptotic approach (AAM) makes it possible to reduce the computational cost of refined models without affecting their accuracies. AAM examples can be found in [32] for plates, or in [36] for shells. In the following, the AAM is described, the Best Theory Diagram (BTD) for shells is introduced and then a method to build the BTD is explained.

5.1 The axiomatic/asymptotic method

The AAM is a tool to build reduced refined models, and it consists of the following steps:

1. Parameters such as the geometry, BCs, materials and layer layouts are fixed.

2. A set of output parameters is chosen, such as displacement or stress components; in the following analyses $\sigma_{\alpha\alpha}$ or u_z were considered.

3. A starting theory is fixed (axiomatic part); that is, the displacement variables to be analyzed are defined; usually, a theory which provides 3D-like solutions is chosen; a reference solution is defined (in the present work the LD4 was adopted, since this fourth-order model offers an excellent agreement with the three-dimensional solutions as highlighted in [29, 32]).

4. The CUF is used to generate the governing equations for the theories considered.

5. The effectiveness of each term of the adopted expansion is evaluated by evaluating the error due to its deactivation; a term is considered as non-effective if the error is negligible;

the deactivation of a term is obtained by means of a penalty technique.

6. The most suitable structural model for a given structural problem is then obtained by discarding all the non-effective variables.

A graphical notation was introduced to show the results. This consists of a table with three lines, and a number of columns equal to the number of the displacement variables used in the expansion. As an example, an LD4 model for a two layer shell is shown in Table 1. Table 2 shows the reduced model in which the first layer term u_{z2} and the second layer term $u^2_{\alpha 2}$ are deactivated. The meaning of the symbols reported in Table 2 is reported in Table 3. The symbol ■ is used to denote the terms that cannot be deactivated in the LW since this would introduce an extra constraint.

5.2 The Best Theory Diagram

It is possible to associate to each reduced refined model the number of the active terms and its error computed with respect to a reference solution as reported in Fig. 3. Errors are reported on the abscissa and the number of active terms is reported on the ordinate. Each black dot represents a reduced refined model and its position on the Cartesian plane is defined considering its error and the number of the active terms. Furthermore, the graphical representation of the active/non-active terms is reported for some reduced models. It is possible to note that some of them present the lowest error for a given number of active terms. These models are labeled in Fig. 3 as 1, 2, 3, 4, 5 and they represent the Pareto front for the considered problem. This Pareto front is defined as the Best Theory Diagram (BTD). This curve can be constructed for several problems, for example by considering several type of materials, geometries and boundary conditions. Moreover, the information reported in a BTD makes it possible to evaluate the minimum number of terms, N_{min}, that have to be used in order to achieve the desired accuracy.

5.3 BTD construction by means of genetic algorithms

The number of all possible combinations of active/not-active terms for a given refined model is equal to 2^M where M is the number of the terms of a model. In the case of an ESL model, M can be computed as $M = 3\,(N+1)$. In the case of an LW model M is computed as $M = 3\,N_l\;(N-1)$. As the expansion order increases, the number of the combinations to consider also increases. A genetic algorithm was used to construct a BTD with a small computational effort.

Each shell theory was considered as an individual. The genes are the terms of the expansion and each gene can be active or not active, as shown in Fig. 4. The meaning of the symbols ▲ and △ is reported in Table 3. Each individual is, therefore, described by the number of active terms and its error computed with respect to a reference solution. Through these two parameters, it is possible to apply the dominance rule in order to evaluate the individual fitness. The generation of new refined theories starting from a generic population is inspired to the reproduction of bacteria; for each individual (i.e. for each shell theory) a number of copies are created according to its dominance and then, a number of mutations are applied in order to vary the set of new individuals. The purpose of this analysis is to find the individuals that belong to the Pareto front, that is, the subset of individuals that are dominated by no other individuals. In all cases, the number of generations, i.e. iterations, needed is equal to 10 and the number of the initial population is equal to 400. The error of the reduced models with respect to a reference solution is evaluated through the following formula:

$$e = 100\,\frac{\sum_{i=1}^{N_p} |Q^i - Q^i_{\mathrm{ref}}|}{\max Q_{\mathrm{ref}}} \cdot \frac{1}{N_p} \tag{30}$$

where Q can be a stress or displacement component, and N_p is the number of points along the thickness on which Q is evaluated.

6 Results

Metallic and composite shells were investigated. A transverse distributed load was considered,

$$p_z = p_z^0 \sin\left(\frac{\pi\, m\, \alpha}{a}\right) \sin\left(\frac{\pi\, n\, \beta}{b}\right) \tag{31}$$

The parameters m and n as well as the surface in which the load is applied (top or bottom) are different for each case.

6.1 Metallic shell

A metallic shell was first considered with $a/R_\beta = 10$, $b/R_\beta = \pi/3$. Thin and thick shells were considered, R_β/h equal to 100 and 4, respectively. The material properties are $E = 73$ GPa and $\nu = 0.34$. Unless otherwise stated, $m = 0$ and $n = 1$. The load was applied on the top surface. The LD4 was used as the reference model for the axiomatic/asymptotic analysis and the BTD. This model was chosen since it provides 3D-like accuracy as shown in previous works by the first author [29, 32]. Some values of the displacement u_z and stress $\sigma_{\alpha\alpha}$ that were evaluated by means of the ED4 and LD4 are reported in Table 4.

The BTD was first built by considering all the combinations given by the 15 displacement variables of the ED4; that is, $2^{15} = 32768$. The BTD was obtained by considering $\sigma_{\alpha\alpha}$, and it is shown in Fig. 5. The BTD, or the Pareto front, was obtained by considering the reduced models that offer the lowest possible error for a given number of active terms. The BTD that was obtained by means of the genetic approach is reported in the same plot. A perfect match was found between these two BTDs. The genetic algorithm evaluated around 400 individuals for 10 generations, this means that only about 4000 out of 32768 theories were evaluated. In this structural problem, the BTD has no reduced models with more than 6 degrees of freedom (DOFs). In other words, it is not possible to achieve higher accuracies with higher computational

costs. However, in this case, the accuracy given by the ED4 models is extremely similar to the one provided by the LD4. It is also interesting to see how for some error ranges there are no reduced models. In this case, four regions were found with no reduced models. This means that some accuracies are not detectable by any reduced model. Figure 6 shows the BTD for the thin and thick shell together with some classical models. In particular, CLT, FSDT and the Pandya model (see Eq. 15) are compared with the BTD. These models are less accurate than the BTD models, particularly in the thick case. This means that it is possible to detect $\sigma_{\alpha\alpha}$ with the same computational cost but higher accuracy than CLT, FSDT and the Pandya model. Or, on the other hand, a better rearrangement of the displacement variables allows one to obtain results as accurate as those from these models without an increase of the degrees of freedom. A detailed analysis of these models is presented in Table 5 in which the accuracies of classical and BTD models are compared. Such a table can be useful in the understanding of how to improve the accuracies of classical models. As an example, the accuracy of the Pandya model for a thin shell can be significantly improved without adding displacement variables by considering the fourth-order terms along the β and z directions and by neglecting all terms that belong to the α direction. In the case of the thick shell, a 6-DOFs model can provide a higher accuracy than the Pandya model. This means that, in some cases, better results can be obtained with reduced models that have a lower number of degrees of freedom than the classical models. The $\sigma_{\alpha\alpha}$ distribution along the thickness is shown in Figure 7. FSDT and Pandya models were considered together with the reference full LD4 solution and the reduced refined models 9T, 6T and 5T that were given in Table 5. The distribution that was computed via the BTD models is more accurate than the distribution computed by means of the classical models in the thick shell case.

It is important to underline that this result is also due to the particular loading case considered that makes the displacement variables along α useless. Table 6 shows some reduced models for

$m = 1$, $n = 1$. Figure 8 shows the BTD for different loading conditions. It can be seen how, in this case, expansion terms along all the three directions are necessary and how the BTD is influenced by the loading conditions to a great extent.

The axiomatic/asymptotic analysis of the metallic shell suggests that

- Genetic algorithms can be used to build the BTD in a more efficient way than by investigating the accuracy of all the shell models that stem from the combinations of the displacement variables.

- The BTD is influenced to a great extend by the geometrical and loading characteristics of the shell. This means that the set of active displacement variables cannot be easily defined a priori. The combined use of the CUF and the axiomatic/asymptotic analysis can represent a tool to build such models and to outline guidelines to select the most relevant terms of the expansion.

- The shell models that belong to the BTD are often more efficient than classical models. In other words, either the BTD models are as accurate as classical models, but less computational expensive or they provide higher accuracy with the same computational cost.

- In some cases, reduced models that provide a given accuracy do not exist, that is, in some accuracy ranges there are not reduced models.

6.2 Laminated shell

Composite laminated shells are dealt with in this section. First the LD4 model capabilities are compared with a 3D elasticity solution by Varadan and Bhaskar [17]. The material properties are $E_L/E_T = 25$, $\nu = 0.25$, $G_{LT}/E_T = G_{TT}/E_T = 0.5$, $G_{Lz}/E_T = 0.2$ and the dimensions of the shell are $a = 4\,R_\beta$ and $b = 2\,\pi\,R_\beta$. The transverse pressure load is applied internally, m

and n are equal to 1 and 4, respectively. The results are given in Table 7. The LD4 results are in excellent agreement with those in [17]. The LD4 was then chosen as the reference model for the axiomatic/asymptotic analysis ad the BTD.

BTDs were first obtained for the symmetric layout, 90°/0°/90°. An ED4 model was first considered. Figure 9 shows the BTD for the $\sigma_{\alpha\alpha}$ in the thick shell case. The BTD was obtained by means of the genetic algorithm, and it perfectly matches the boundaries of the best accuracy models that were computed by considering all the combinations ($2^{15} = 32768$) of the ED4 displacement variables. As for the metallic shell case, some empty regions were found; they are labeled as 1 and 2. This means that for some error intervals, and for some number of DOFs it is not possible to construct any reduced models. The minimum error that can be obtained through the ED4 terms with respect to LD4 is about 3.5% with 11 displacement variables. The remaining four variables are not able to improve this result. Figure 10 shows the BTDs that were obtained by considering u_z and $\sigma_{\alpha\alpha}$, thin and thick shells were investigated. Both the thickness and the considered outputs influence the BTD to a great extent. The accuracy of CLT, FSDT and Pandya models are compared with BTD in Fig. 11. In the most cases, these models are far from the BTD. This means that with the same number of degrees of freedom, better accuracies can be achieved and that the same accuracy can be achieved with fewer displacement variables. Table 8 shows the accuracy of the models from the open literature and that one from some of the models that belong to the BTD. Such a table can provide some guidelines to improve the accuracy of classical models. For instance, the accuracy of the FSDT model in detecting $\sigma_{\alpha\alpha}$ for a thin shell analysis can be improved by considering a third-order term instead of a first-order term (i.e. $u_{\beta 4}$ instead of $u_{\beta 2}$). Stress $\sigma_{\alpha\alpha}$ and displacement u_z distributions along the thickness are reported in Fig. 12, the reduced models of Table 8 are employed, and the reference solution is the full LD4 model. It is confirmed that the BTD 9T model provides the best accuracy although the match with the LD4 model is not perfect.

Figure 13 shows BTDs based on LD4 models. u_z and $\sigma_{\alpha\alpha}$ were considered. As it was already found in the ED4 case, BTDs are influenced by the output variable and the shell geometry. On the other hand, BTDs for LD4 have a narrower error range than ESL. This means that by only considering the twelve to, bottom and interface variables, that is, those displacement variables that cannot be deactivated, the accuracy of the reduced LD4 models is high. The error, in fact, is lower than 2.5 % in the thick shell case. Table 9 presents some reduced models that have a fixed number of variables (18). A defined set of higher-order terms on the top and bottom layers are needed to have a good accuracy. On the other hand, it is more difficult to define a fixed set of higher-order terms along the middle layer. The $\sigma_{\alpha\alpha}$ distribution along the thickness is shown in Fig. 14. The reduced models of Table 9 are compared with the full LD4 solution. The reduced model distributions match the full LD4 one perfectly.

An asymmetric layout, $0°/90°$ was considered as the second assessment for the composite shell case. The LD4 was used as the reference solution. ED4 models were first investigated. Figure 15 shows BTD for $\sigma_{\alpha\alpha}$, and the classical model accuracy was also included. Unlike the previous cases, classical models are close to the BTD except the Pandya model in the thick shell case. This means that these models provide the best accuracy possible for a given number of DOFs. Table 10 shows the accuracy of the classical models and of the BTD models that have the same amount of DOFs. The linear and parabolic terms in z play a fundamental role in the refinement of the Pandya model. Figure 16 present a comparison between the BTD for $\sigma_{\alpha\alpha}$ and the one for u_z. As in all the previous cases, significant differences in the BTD for different outputs are observable. Figure 17 shows the $\sigma_{\alpha\alpha}$ distribution along the thickness via the reduced models of Table 10 and the full LD4 model. The BTD 9T model perfectly matches the full LD4 solution. The BTD for the asymmetric composite shell based on the LD4 is shown in Fig. 18 with all the reduced models that were obtained by considering all the possible term combinations ($2^{18} = 262144$) of a two-layer LD4. It is possible to note that the genetic approach can detect

almost all the models that lie on the BTD. Figure 19 shows BTDs for $\sigma_{\alpha\alpha}$ and u_z for thin and thick shells. As in the symmetric case, the BTD based on LD4 has a narrower error range than the ED4 one.

The analyses that were carried out on the composite shells suggest the following:

- BTDs are influenced to a great extent by the geometry, the stacking sequence and the considered displacement/stress component.
- The application of the axiomatic/asymptotic method leads to reduced layer-wise models that can have much fewer displacement variables than the full models. The reduction in computational costs is much more evident in layer-wise than in equivalent single layer models.
- The genetic algorithm approach is a valid tool to build BTD.
- Classical models are often qui far from the BTD curve. This means that they can be improved both in accuracy and computational cost standpoint.

7 Conclusion

This paper has dealt with the axiomatic/asymptotic method (AAM) of isotropic and composite shells. The AAM can be seen as a tool to evaluate the influence of each unknown variables on the solution, and it leads to the definition of reduced models that have fewer DOFs than the full models without accuracy loss. The systematic use of the AAM has led to the Best Theory Diagram (BTD). The BTD is a curve in which the computationally cheapest structural model can be read for any accuracy level. In other words, given an error with respect to an exact, or quasi exact solution, the BTD provides the smallest set of unknown variables that can fulfill such a requirement. The results have been obtained for different boundary conditions, materials

and geometries. Navier-type, closed-form solutions have been employed.

The following main conclusions can be drawn:

1. BTDs are influenced to a great extent by the geometry of the shell, the loading conditions, the material properties and by the quantity considered (displacement/stress component).

2. Often, classical models do not belong to the BTD. This means that the BTD models are either as accurate as classical models, but less computational expensive or they provide higher accuracy with the same computational cost.

3. The influence of a displacement variable on the solution is extremely related to the problem characteristics. Furthermore, it is not possible to foresee the importance of most of the variables. The systematic exploitation of the AAM can be seen as a tool to evaluate each variable; that is, to assess the accuracy of any structural model against a reference solution.

4. The AAM is particularly efficient in the layer-wise case in which a substantial reduction of the number of variables was achieved.

Future works should deal with multifield problems and mixed variational models.

References

[1] G. Kirchhoff. "Uber das gleichgewicht und die bewegung einer elastischen scheibe" *Journal fur reins und angewandte Mathematik* , 40:51–88, 1850. doi: 10.1515/crll.1850.40.51.

[2] A. E. H. Love. *A Treatise on the Mathematical Theory of Elasticity.* Cambridge University Press, Cambridge, 1892.

[3] H. Kraus. *Thin Elastic Shells.* John Wiley & Sons, 1967.

[4] E. Reissner. The effect of transverse shear deformation on the bending of elastic plates. *Journal of Applied Mechanics*, 12:69–76, 1945.

[5] R.D. Mindlin. Influence of rotatory inertia and shear in flexural motions of isotropic elastic plates. *Journal of Applied Mechanics*, 18:1031–1036, 1951.

[6] B.F. Vlasov. On the equations of Bending of plates. *Dokla Ak. Nauk. Azerbeijanskoi-SSR*, 3:955–979, 1957.

[7] J. N. Reddy. *Mechanics of Laminated Plates, Theory and Analysis*. CRC Press, Boca Raton, 1997.

[8] W.T. Koiter. A consistent first approximation in the general theory of thin elastic shells. In *Proc. of Symp. on the Theory of Thin Elastic Shells*, Noth-Hollad, Amsterdam, August 1959.

[9] F.B. Hildebrand, E. Reissner, and Thomas G.B. Notes in the foundations of the theory of small displacement of orthotropic shells. Technical report, NASA, March.

[10] E. I. Grigolyuk and Kogan F.A. The present status of the thoery of multilayered shells. *Prikl. Mekh.*, 8:3–17, 1972.

[11] R.K. Kapania. A review on the analysis of laminated shells. *ASME J. Pressure Vessel Technol.*, 111(2):88–96, 1989. doi: 10.1515/crll.1850.40.51.

[12] E. I. Grigolyuk and G. M. Kulikov. General directions of the development of theory of shells. *Mechanics of Composite Materials*, 24(2):231–241, 1988. doi: 10.1515/crll.1850.40.51.

[13] A. K. Noor, W. S. Burton, and C. W. Bert. Computational model for sandwich panels and shells. *Applied Mechanics Reviews*, 49(3):155–199, 1996. doi: 10.1115/1.3101923.

[14] O. A. Fettahlioglu and C. R. Steele. Asymptotic solutions for orthotropic nonhomogeneous shells of revolution. *Journal of Applied Mechanics*, 41(3):753–758, 1974. doi: 10.1115/1.3423383.

[15] V. L. Berdichevsky. Variational-asymptotic method of shell theory construction. *Prikladnaya Matematika i Mekhanika*, 43:664–667, 1979.

[16] V. L. Berdichevsky and V. Misyura. Effect of accuracy loss in classical shell theory. *Journal of Applied Mechanics*, 59(2):217–223, 1992. doi: 10.1115/1.2899492.

[17] T.K. Varadan and K. Bhaskar. Bending of laminated orthotropic cylindrical shells - an elasticity approach. *Composite Structures*, 17:141 – 156, 1991.

[18] T. Hsu and J.T. Wang. A theory of laminated cylindrical shells consisting of layers of orthotropic laminae. *AIAA Journal*, 8:2141–2146, 1970.

[19] T. Hsu and J.T. Wang. Rotationally Symmetric Vibrations of Orthotropic Layered Cylindrical Shells. *Journal of Sound and Vibration*, 16:473–487, 1970.

[20] Y.K. Cheung and C.I. Wu. Free Vibrations of Thick, Layered Cylinders Having Finite Length with Various Boundary Conditions. *Journal of Sound and Vibration*, 24:189–200, 1972.

[21] S. Srinivas. A refined analysis of composite laminates. *Journal of Sound and Vibration*, 30:495–507, 1973.

[22] K.N. Cho, C.W. Bert and A.G. Striz. Free Vibrations of Laminated Rectangular Plates Analyzed by Higher order Individual-Layer Theory. *Journal of Sound and Vibration*, 145:429–442, 1991.

[23] D.H. Robbins Jr. and J.N. Reddy. Modeling of thick composites using a layer-wise theory. *International Journal for Numerical Methods in Engineering*, 36:655–677, 1993.

[24] S.G. Lekhnitskii. Strength Calculation of Composite Beams. *Vestnik Inzhen. i Tekhnikov*, 9, 1935.

[25] S. A. Ambartsumian. On a theory of bending of anisotropic plates. *Investiia Akad. Nauk SSSR*, 4, 1958.

[26] E. Reissner. On a certain mixed variational theory and a proposed application. *International Journal for Numerical Methods in Engineering*, 20:1366-1368, 1984.

[27] H. Murakami. Laminated composite plate theory with improved in-plane responses. *Journal of Applied Mechanics*, 53:661-666, 1986.

[28] E. Carrera. Mixed Layer-Wise Models for Multilayered Plates Analysis. *Composite Structures*, 43:57-70, 1998.

[29] E. Carrera. Theories and finite elements for multilayered plates and shells: A unified compact formulation with numerical assessment and benchmarking. *Arch. Comput. Meth. Engng*, 10(3):215–296, 2003.

[30] E. Carrera and M. Petrolo. On the Effectiveness of Higher-Order Terms in Refined Beam Theories. *Journal of Applied Mechanics*, 78:1–17, 2011.

[31] E. Carrera, F. Miglioretti and M. Petrolo. Computations and evaluations of higher-order theories for free vibration analysis of beams. *Journal of Sound and Vibration*, 331:4269–4284, 2012.

[32] E. Carrera and M. Petrolo. Guidelines and recommendation to contruct theories for metallic and composite plates. *AIAA Journal*, 48(12):2852–2866, 2010. doi: 10.2514/1.J050316.

[33] E. Carrera, F. Miglioretti and M. Petrolo. Accuracy of refined finite elements for laminated plate analysis. *Composite Structures*, 93:1311–1327, 2011.

[34] E. Carrera, F. Miglioretti and M. Petrolo. Guidelines and recommendations on the use of higher order finite elements for bending analysis of plates. *International Journal for Computational Methods in Engineering Science and Mechanics*, 12(6):303–324, 2011. doi:10.1080/15502287.2011.615792.

[35] E. Carrera and F. Miglioretti. Selection of appropriate multilayered plate theories by using a genetic like algorithm. *Composite Structures*, 94(3):1175–1186, 2012. doi: http://dx.doi.org/10.1016/j.compstruct.2011.10.013.

[36] D. S. Mashat, E. Carrera, A. M. Zenkour, and S. A. Al Khateeb. Use of axiomatic/asymptotic approach to evaluate various refined theories for sandwich shells. *Composite Structures*, 109:139–149, 2014. doi: http://dx.doi.org/10.1016/j.compstruct.2013.10.046.

[37] D. S. Mashat, E. Carrera, A. M. Zenkour, and S. A. Al Khateeb. Axiomatic/asymptotic evaluation of multilayered plate theories by using single and multi-points error criteria. *Composite Structures*, 106(0):393–406, 2013. doi: http://dx.doi.org/10.1016/j.compstruct.2013.05.047.

[38] M. Petrolo and A. Lamberti. Asymptotic/axiomatic analysis of refined layer-wise theories for composite and sandwich plates. *Mechanics of Advanced Materials and Structures*, In Press.

[39] E. Carrera and A. Lamberti and F. Miglioretti and M. Petrolo. Best Theory Diagram for Metallic and Laminated Composite Plates. Submitted.

[40] A.W. Leissa. *Vibration of shells.* Ohio State University, Columbus, Ohio, USA, 1973. NASA SP-288.

[41] E. Carrera and S. Brischetto. Analysis of thickness locking in classical, refined and mixed multilayered plate theories. *Composite Structures*, 82(4):549 – 562, 2008. doi: http://dx.doi.org/10.1016/j.compstruct.2007.02.002.

[42] B. Pandya and T. Kant "Finite element analysis of laminated composite plates using high-order displacement model" *Compos Sci Technol* , 32:137–55, 1988.

[43] E. Carrera, S. Brischetto, and P. Nali. *Plates and Shells for Smart Structures Classical and Advanced Theories for Modeling and Analysis.* John Wiley & Sons, Inc., 2011.

[44] E. Carrera, M. Cinefra, M. Petrolo and E. Zappino. *Finite Element Analysis of Structures through Unified Formulation.* John Wiley & Sons, Inc., 2011.

Tables

■	▲	▲	▲	■	▲	▲	▲	■
■	▲	▲	▲	■	▲	▲	▲	■
■	▲	▲	▲	■	▲	▲	▲	■

Table 1: Representation of the full model.

■	▲	▲	▲	■	△	▲	▲	■
■	▲	▲	▲	■	▲	▲	▲	■
■	△	▲	▲	■	▲	▲	▲	■

Table 2: Representation of the reduced model.

Active term	Inactive term	Non-deactivable term
▲	△	■

Table 3: Symbols to indicate the status of a displacement variable.

$\overline{u}_z(z=0)$	$\overline{\sigma}_{\alpha\,\alpha}(z=\mp h/2)$	$\overline{u}_z(z=0)$	$\overline{\sigma}_{\alpha\,\alpha}(z=\mp h/2)$
LD4			
$R_\beta/h=100$		$R_\beta/h=4$	
1.6669	−2.5757	2.1213	−3.3373
	2.5504		2.7722
ED4			
$R_\beta/h=100$		$R_\beta/h=4$	
1.6669	−2.5757	2.1132	−3.3236
	2.5504		2.7882

Table 4: ED4 and LD4 reference stress and displacement values for the isotropic shell, $\overline{u}_z = \frac{10\,u_z\,E_L\,h^3}{p_0\,R_\beta^4}$, $\overline{\sigma}_{\alpha\,\alpha} = \frac{10\,\sigma_{\alpha\,\alpha}}{p_0\,(R_\beta/h)^2}$.

	$R_\beta/h=100$			
	Pandya, $M_e/M=9/15$	BTD, $M_e/M=9/15$ (9T)	FSDT, $M_e/M=5/15$	BTD, $M_e/M=5/15$ (5T)
	▲▲▲▲△ ▲▲▲▲△ ▲△△△△	△△△△△ ▲▲△▲▲ ▲▲▲▲▲	▲▲△△△ ▲▲△△△ ▲△△△△	△△△△△ ▲▲△▲△ ▲▲△△△
Error	1.6074 %	3.9210×10^{-6} %	0.1465 %	0.1072 %
	$R_\beta/h=4$			
	Pandya, $M_e/M=9/15$	BTD, $M_e/M=6/15$ (6T)	FSDT, $M_e/M=5/15$	BTD, $M_e/M=5/15$ (5T)
	▲▲▲▲△ ▲▲▲▲△ ▲△△△△	△△△△△ ▲▲△△△ ▲▲▲▲△	▲▲△△△ ▲▲△△△ ▲△△△△	△△△△△ ▲▲△△△ ▲△▲▲△
Error	3.1428 %	0.6014 %	3.2831 %	1.3366 %

Table 5: Accuracy of classical and BTD models for the isotropic shell, ED4

	$R_\beta/h = 100$ $M_e/M = 6/15$	$R_\beta/h = 4$ $M_e/M = 12/15$
	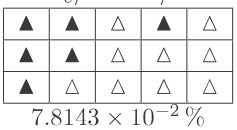	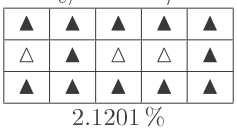
Error	$7.8143 \times 10^{-2}\,\%$	$2.1201\,\%$

Table 6: Reduced models for the isotropic shell, $m = n = 1$.

	$90^\circ/0^\circ$		$90^\circ/0^\circ/90^\circ$	
	$\overline{u}_z$ $(z = 0)$	$\overline{\sigma}_{\alpha\,\alpha}$ $(z = \mp h/2)$	$\overline{u}_z$ $(z = 0)$	$\overline{\sigma}_{\alpha\,\alpha}$ $(z = \mp h/2)$
		$R_\beta/h = 4$		
Ref. [17]	6.100	-0.9610	4.009	-0.2701
		0.2120		0.1270
L4	6.100	-0.9614	4.009	-0.2721
		0.2088		0.1267
		$R_\beta/h = 100$		
Ref. [17]	1.367	2.300	0.4715	0.0018
		0.1871		0.0838
L4	1.367	2.300	0.4715	0.0018
		0.1871		0.0838

Table 7: Displacement and stress for the composite shell, LD4 vs. the Varadan and Bhaskar solution [17], $\overline{u}_z = \frac{10\,u_z\,E_L\,h^3}{p_0\,R_\beta^4}$, $\overline{\sigma}_{\alpha\,\alpha} = \frac{10\,\sigma_{\alpha\,\alpha}}{p_0\,(R_\beta/h)^2}$.

	$\sigma_{\alpha\alpha}$		u_z	
		$R_\beta/h = 100$		
	Pandya, $M_e/M = 9/15$	BTD, $M_e/M = 9/15$ (9T)	Pandya, $M_e/M = 9/15$	BTD, $M_e/M = 9/15$ (9T)
	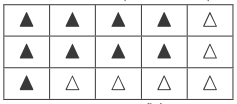	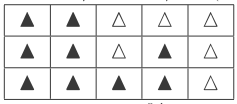	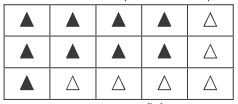	
Error	$0.1201\,\%$	$0.0547\,\%$	$0.2485\,\%$	$0.0771\,\%$
		$R_\beta/h = 4$		
	Pandya, $M_e/M = 9/15$	BTD, $M_e/M = 6/15$ (6T)	Pandya, $M_e/M = 9/15$	BTD, $M_e/M = 9/15$ (9T)
	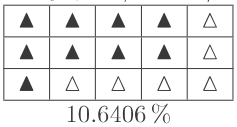	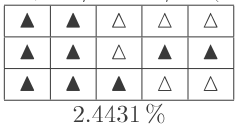	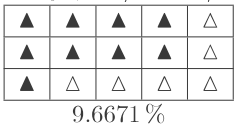	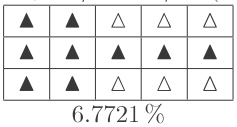
Error	$10.6406\,\%$	$2.4431\,\%$	$9.6671\,\%$	$6.7721\,\%$
	FSDT, $M_e/M = 5/15$	BTD, $M_e/M = 5/15$ (5T)	FSDT, $M_e/M = 5/15$	BTD, $M_e/M = 5/15$ (5T)
	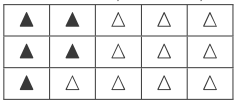		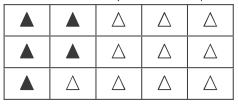	
Error	$13.9300\,\%$	$10.6558\,\%$	$27.6149\,\%$	$8.5433\,\%$

Table 8: Accuracy of classical and BTD models for the symmetric composite shell, ED4.

	T_1	T_2
		
Error	$0.2723\,\%$	$1.3126\,\%$

Table 9: Reduced models for the symmetric composite shell with $M_e/M = 18/39$, LD4 models, $\sigma_{\alpha\alpha}$, $R_\beta/h = 4$.

	$R_\beta/h = 100$	
	Pandya, $M_e/M = 9/15$	BTD, $M_e/M = 9/15$ (9T)
		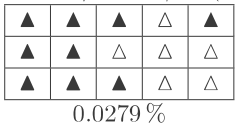
Error	0.0389 %	0.0279 %
	$R_\beta/h = 4$	
	Pandya, $M_e/M = 9/15$	BTD, $M_e/M = 9/15$ (9T)
	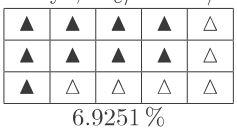	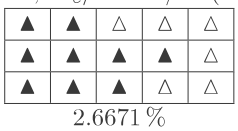
Error	6.9251 %	2.6671 %
	FSDT, $M_e/M = 5/15$	BTD, $M_e/M = 5/15$ (5T)
	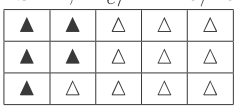	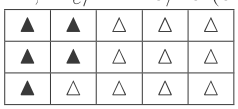
Error	8.4968 %	8.4968 %

Table 10: Accuracy of classical and BTD models for the asymmetric composite shell, ED4, $\sigma_{\alpha\alpha}$.

Figures

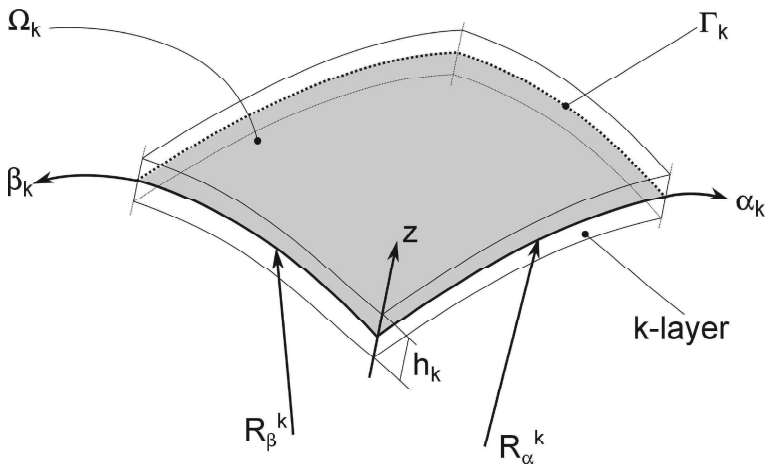

Figure 1: Shell geometry and reference frame.

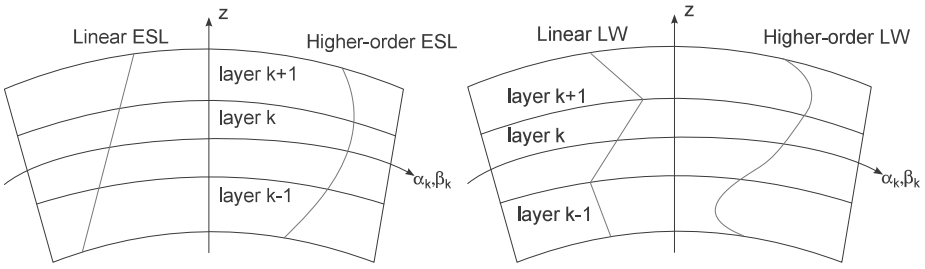

(a) ESL (b) LW

Figure 2: ESL and LW displacement distributions through the shell thickness.

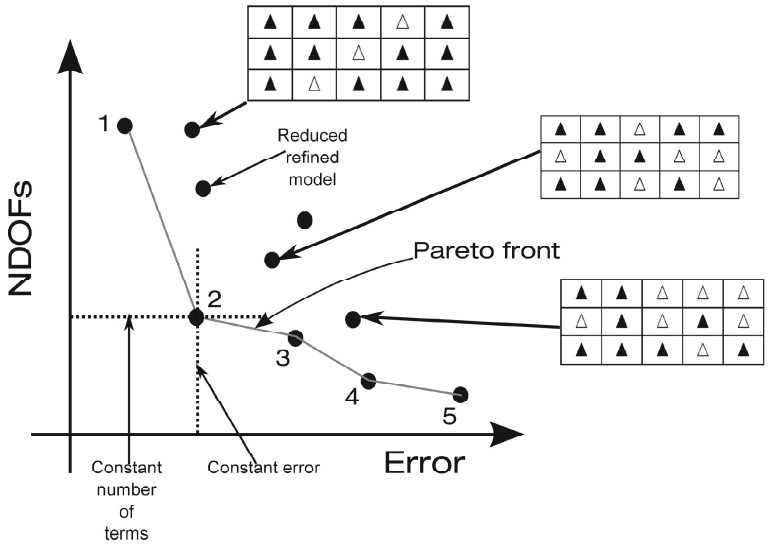

Figure 3: The Best Theory Diagram.

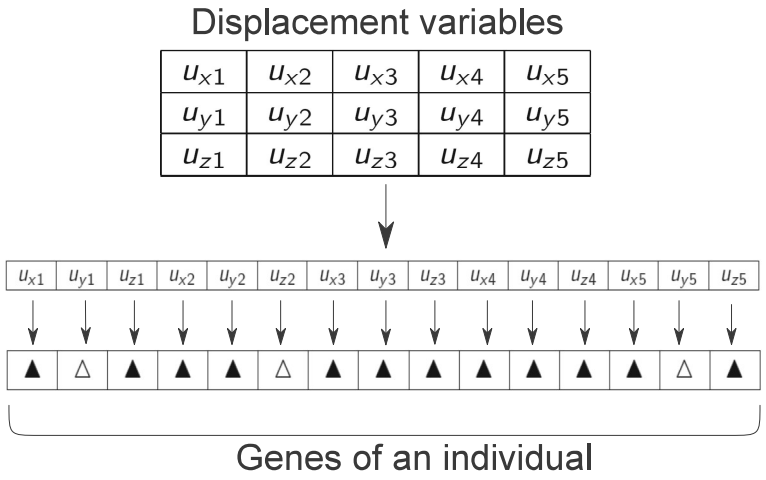

Figure 4: Displacement variables of a refined model and genes of an individual.

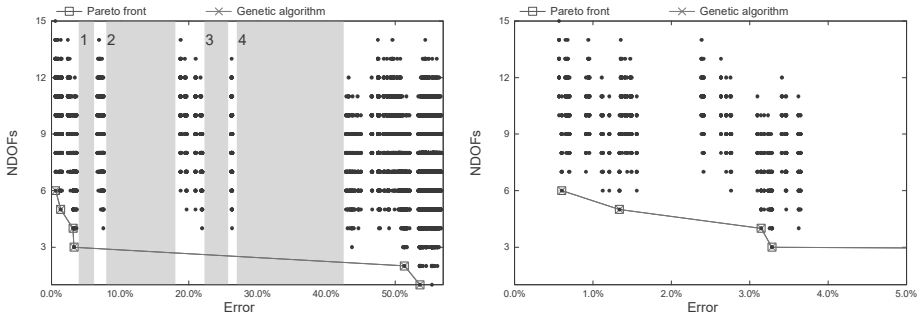

(a) (b)

Figure 5: BTD for the thick isotropic shell and accuracy of all the shell models given by the 2^{15} combinations of the ED4 displacement variables, $R_\beta/h = 4$.

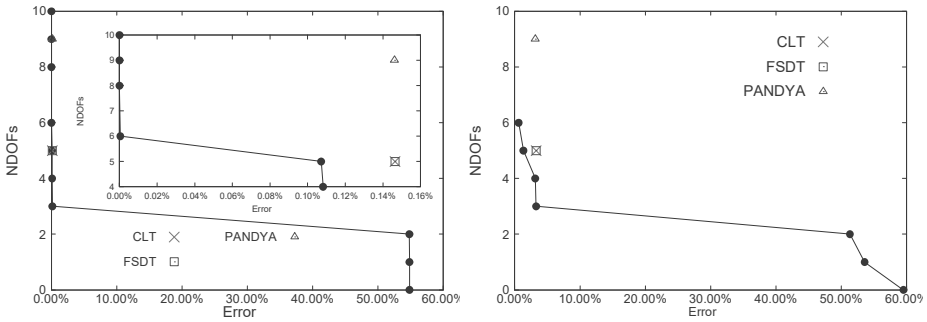

(a) $R_\beta/h = 100$ (b) $R_\beta/h = 4$

Figure 6: BTD and classical model accuracy for the isotropic shell.

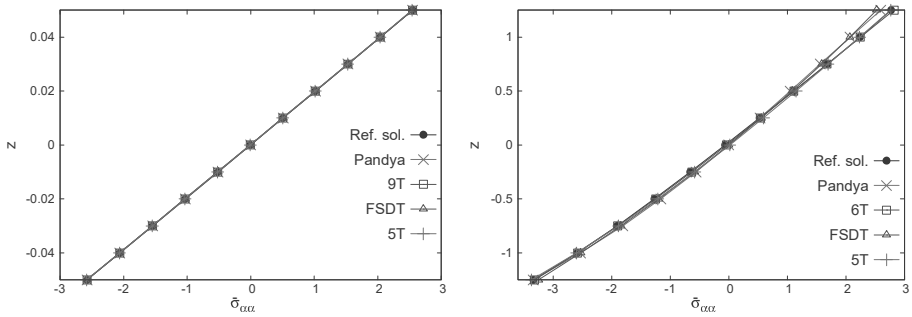

(a) $R_\beta/h = 100$. (b) $R_\beta/h = 4$.

Figure 7: Stress distributions for the isotropic shell via different models.

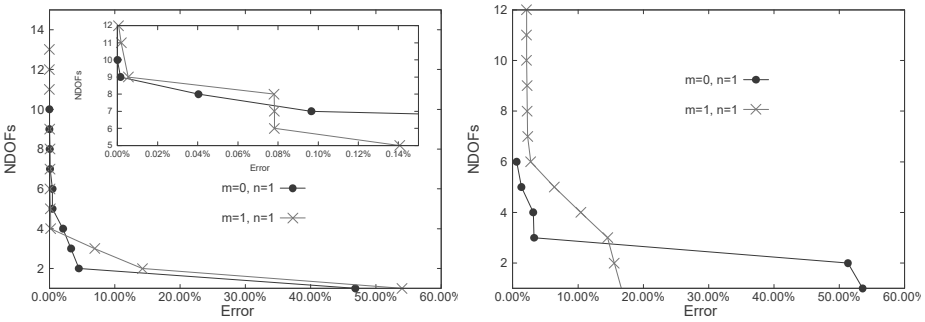

(a) $R_\beta/h = 100$. (b) $R_\beta/h = 4$.

Figure 8: Influence of the loading on the BTD for the isotropic shell.

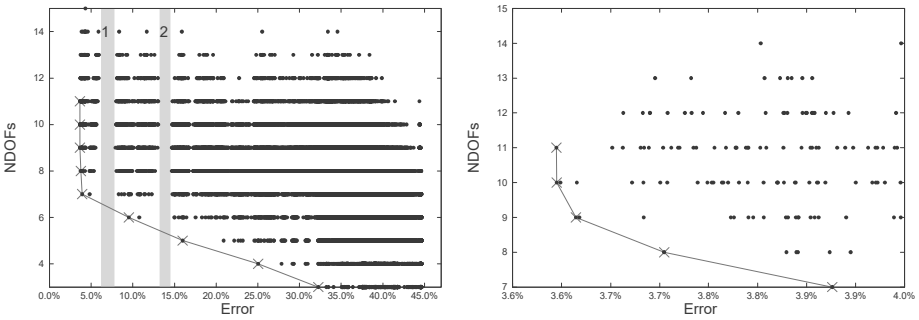

(a) (b)

Figure 9: BTD based on $\sigma_{\alpha\alpha}$ for the symmetric composite shell, $R_\beta/h = 4$, ED4.

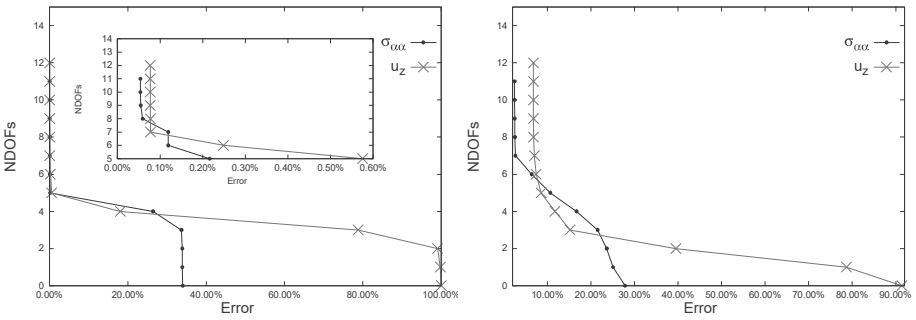

(a) $R_\beta/h = 100$ (b) $R_\beta/h = 4$

Figure 10: BTDs based on u_z and $\sigma_{\alpha\alpha}$ for the symmetric composite shell, ED4.

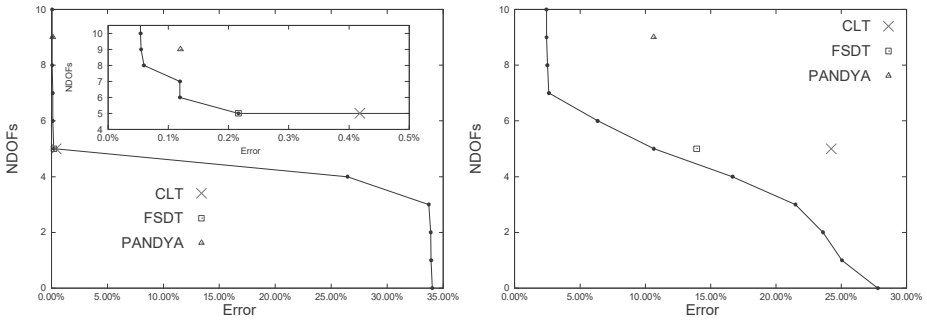

(a) $R_\beta/h = 100$ (b) $R_\beta/h = 4$

Figure 11: Comparison among BTD and other theories for the symmetric composite shell, ED4, $\sigma_{\alpha\alpha}$.

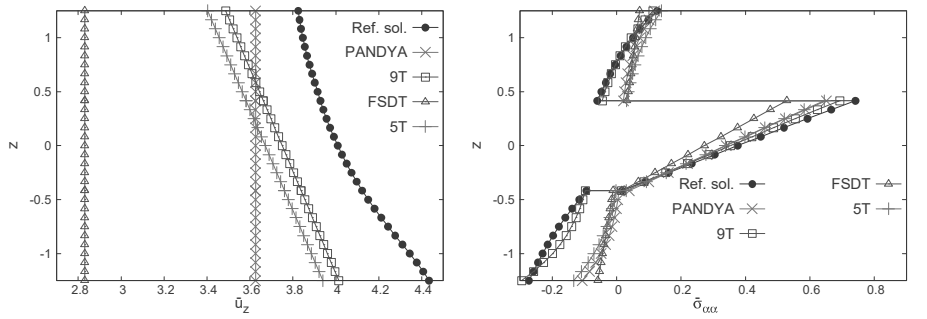

(a) u_z (b) σ_{xx}

Figure 12: Stress $\sigma_{\alpha\alpha}$ and displacement u_z distributions along the thickness for the symmetric composite shell, ED4, $R_\beta/h = 4$.

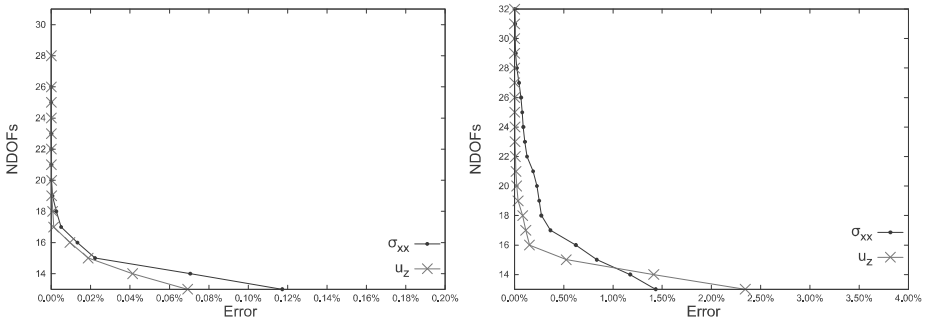

(a) $R_\beta/h = 100$. (b) $R_\beta/h = 4$.

Figure 13: BTD for the symmetric composite shell, LD4.

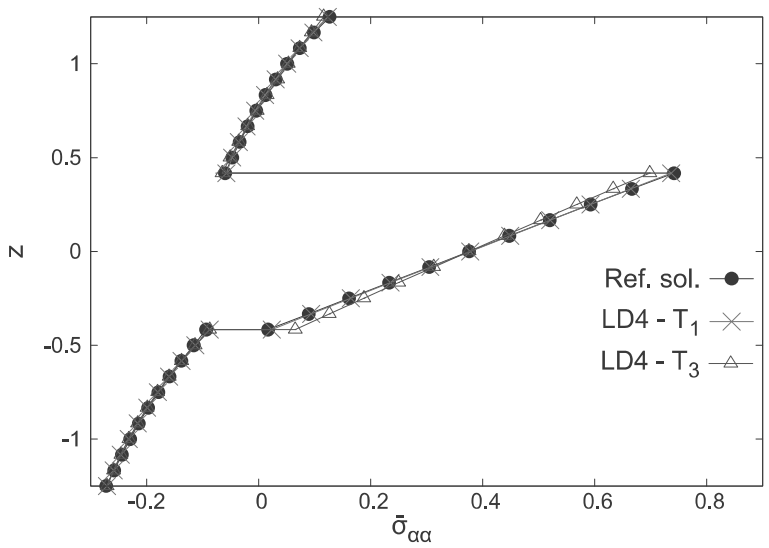

Figure 14: $\sigma_{\alpha\alpha}$ distribution along the thickness via LD4 reduced and full models for the symmetric composite shell, $R_\beta/h = 4$.

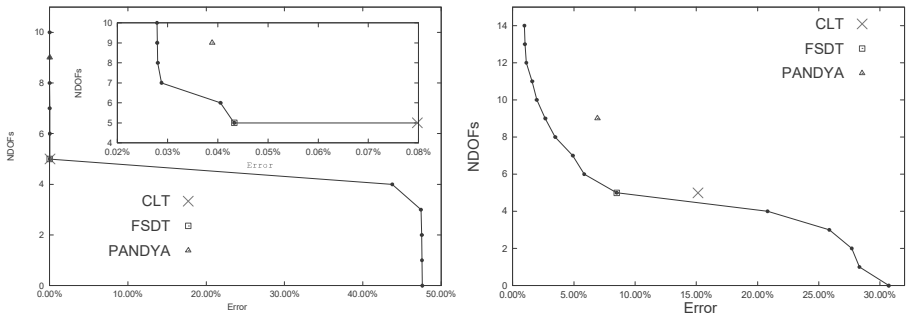

(a) $R_\beta/h = 100$ (b) $R_\beta/h = 4$

Figure 15: BTD for the asymmetric composite shell, ED4 model, $\sigma_{\alpha\alpha}$.

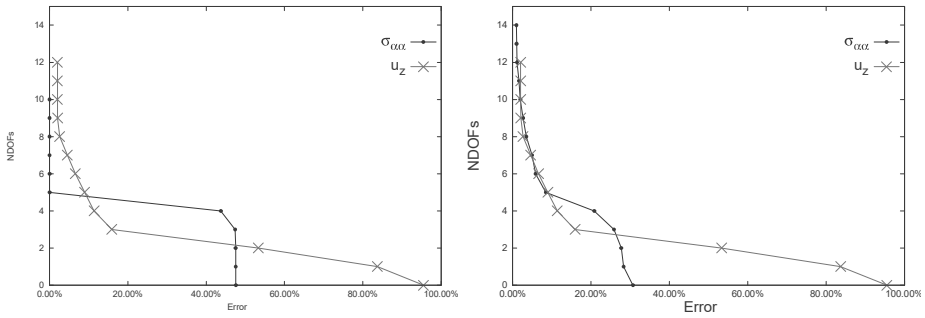

(a) $R_\beta/h = 100$ (b) $R_\beta/h = 4$

Figure 16: BTD for the asymmetric composite shells, ED4, $\sigma_{\alpha\alpha}$ and u_z.

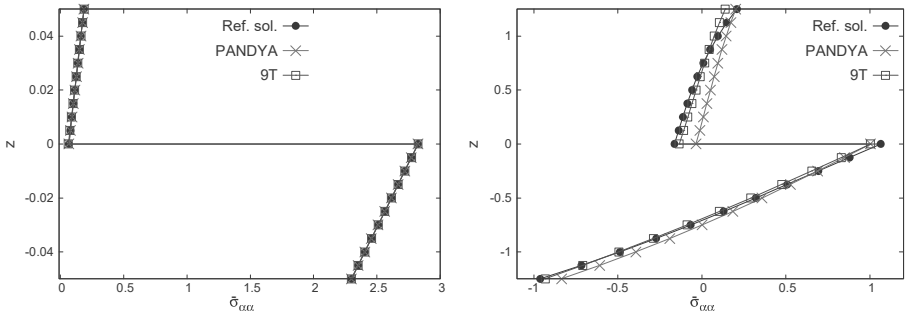

(a) $R_\beta/h = 100$ (b) $R_\beta/h = 4$

Figure 17: $\sigma_{\alpha\alpha}$ distribution along the thickness for the asymmetric composite shell, ED4.

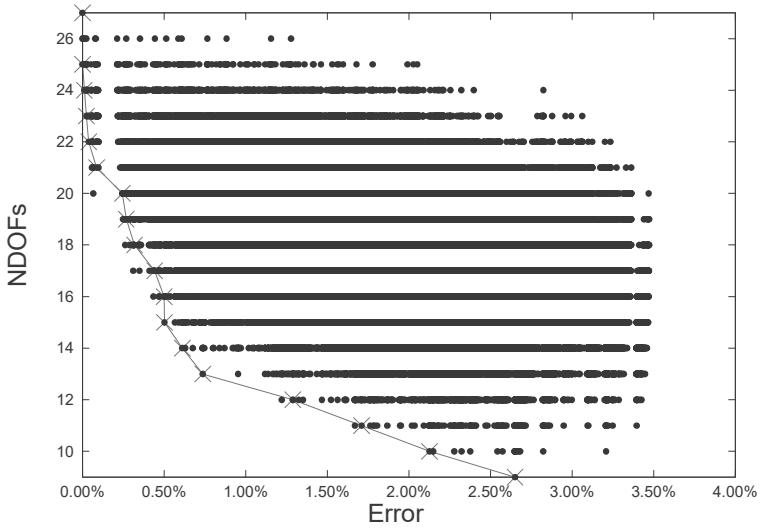

Figure 18: BTD for the asymmetric composite shell, LD4, $\sigma_{\alpha\alpha}$, $R_\beta/h = 4$.

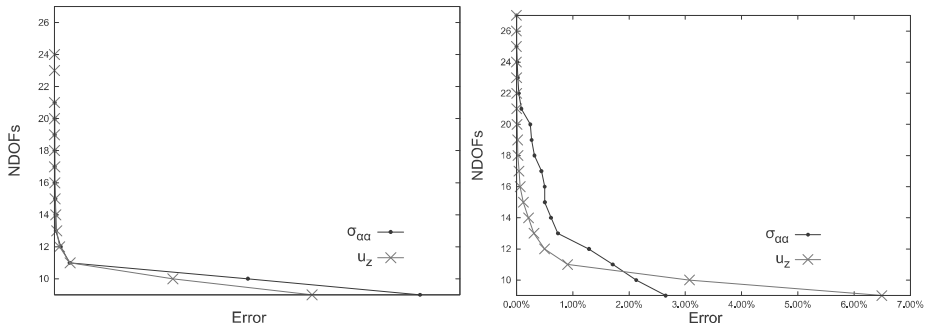

(a) $R_\beta/h = 100$ (b) $R_\beta/h = 4$

Figure 19: BTD for the asymmetric composite shell, LD4 model, u_z and $\sigma_{\alpha\alpha}$.